Detection of the Quantum Capacitance of a Point Contact via Dispersive Gate Sensing

M.C. Jarratt,[1,†] S.J. Waddy,[1,†] A. Jouan,[1] A.C. Mahoney,[1] G.C. Gardner,[2,3] S. Fallahi,[2] M.J. Manfra,[2,3,4] and D.J. Reilly[1,5,*]

[1] *ARC Centre of Excellence for Engineered Quantum Systems, School of Physics, The University of Sydney, Sydney, New South Wales 2006, Australia*

[2] *Department of Physics and Astronomy and Birck Nanotechnology Center, Purdue University, West Lafayette, Indiana 47907, USA*

[3] *Microsoft Quantum Purdue and School of Materials Engineering, Purdue University, West Lafayette, Indiana 47907, USA*

[4] *School of Electrical and Computer Engineering, and School of Materials Engineering, Purdue University, West Lafayette, Indiana 47907, USA*

[5] *Microsoft Quantum Sydney, The University of Sydney, Sydney, New South Wales 2006, Australia*

(Received 4 August 2020; accepted 28 September 2020; published 7 December 2020)

The readout technique of dispersive gate sensing (DGS) uses an electrode embedded in a microwave resonator to detect the quantum capacitance of a mesoscopic device arising from single-electron tunneling. Here, we extend DGS from the detection of discrete tunnel events to the open regime, observing jumps in the capacitance of a quantum point contact (QPC) that arise when the one-dimensional sub-bands populate. We compare the signal from DGS to transport measurements for various QPC geometries, including measurements at finite bias. Unlike traditional charge sensing, which is limited by screening at high density, our results suggest that DGS can also probe the charge configuration of open quantum devices, where electrons are delocalized and multiple sub-bands are occupied.

DOI: 10.1103/PhysRevApplied.14.064021

I. INTRODUCTION

A cornerstone of mesoscopic physics is the quantization of conductance in units of e^2/h, a well-understood phenomenon that arises from the transmission of charge carriers via a discrete number of one-dimensional (1D) sub-bands [1,2]. The quantum capacitance of a 1D system [3,4], although not quantized like its conductance, should similarly exhibit discontinuous jumps with gate voltage as the chemical potential crosses the Van Hove singularity in the density of states (DOS) of each sub-band. The detection of such jumps has proven challenging however, since such measurements typically require attofarad sensitivity in the presence of picofarad-scale (parasitic) capacitance.

A recently explored approach to overcoming this challenge uses the dispersive shift of an LC resonator to detect single-electron tunneling and probe the quantum capacitance of a mesoscale device [5–12]. When applied to a gate electrode [13], dispersive sensing also provides a scalable means of performing single-shot readout of qubits [14,15]. Specifically, the technique works by using a small oscillating gate voltage δv to induce charge δq, which appears as an additional differential capacitive contribution to the resonator $\delta c = \delta q/\delta v$, altering its resonance frequency by an amount $\delta f_0 \sim -\delta c f_0/2C$, where C is the total capacitance.

In this paper, we extend the dispersive-gate-sensing (DGS) technique [13] beyond the detection of single-electron tunneling, showing that it is also well suited to probing the quantum capacitance of an open system, where many electrons are transported via partially or fully transmitting quantum modes. Similar to compressibility measurements [16], quantum capacitance is a thermodynamic quantity that can reveal fundamental information about the charge configuration of a quantum system [17,18]. For instance, using quantum point contacts (QPCs) that are formed in a two-dimensional electron gas (2DEG) as model devices, we show that DGS can detect jumps in the capacitance associated with a 1D system, essentially probing the DOS in the QPC without the use of a transport current or proximal charge sensor [19]. The same DGS approach also reveals the presence of unwanted localized charge states [20] that often form as the QPC is fully depleted. We compare our DGS measurements with conventional transport, including finite-bias spectroscopy, and relate our experiment to a simple model for the quantum capacitance of an ideal 1D system.

*david.reilly@sydney.edu.au

†These authors contributed equally to this work.

Looking to previous measurements of 1D capacitance in micron-scale devices [17], it is perhaps not obvious that the nanoscale constriction of a QPC can be probed using gate sensing. Surprisingly, we show that the technique remains sensitive to the local DOS in a QPC, even in the open regime where the channel is populated by several sub-bands and screening diminishes the sensitivity of conventional charge detectors. Such a regime has recently become of interest for reading out the parity state of a topological qubit by detecting changes in the hybridization of an electron wave function to a quantum dot or reservoir [21,22]. Beyond just the detection of state-dependent single-electron tunneling, our work also highlights the potential for DGS to be used in the tune-up of qubit devices, remaining sensitive to charge states over a range that spans the few-electron tunneling regime to essentially an open quantum system. Since the dynamic range of DGS can cover this full span of operating conditions, the technique may alleviate altogether the need for conventional charge sensors in scaled-up qubit arrays.

II. DETECTING THE QUANTUM CAPACITANCE OF A QPC

Our setup for detecting the quantum capacitance of a QPC is shown in Fig. 1. We examine devices with two distinct gate patterns, as shown in Figs. 1(a) and 1(b). For either device, the application of negative voltages to two Ti-Au gates on the surface of a $GaAs/Al_{0.3}Ga_{0.7}As$ heterostructure forms a QPC in the 2DEG, 91 nm below the surface. All of the devices examined have comparable 2D density and mobility (approximately 1.3×10^{11} cm^{-2} and 3.50×10^{6} cm^2/Vs, respectively). Annealed ohmic contacts, either side of the QPCs, provide source and drain reservoirs for conventional transport measurements, as well as capacitively coupled rf grounds.

For each device, one or more of the gates forming the QPC is also used for dispersive sensing by wire bonding it to an off-chip LC resonator [23], comprising a superconducting Nb-Ti planar spiral inductor $L = 150$ nH for device 1 $L = 400$ nH for device 2 and in resonance with the intrinsic parasitic capacitance of the device [see Fig. 1(c) for a photograph of the off-chip resonator].

The off-chip LC resonator is, in fact, part of a network of resonators, constructed to enable frequency multiplexing of signals from many gates [23]. An Au-Pd resistor and multilayer parallel-plate capacitor form an on-chip bias tee, allowing dc voltages to also be applied to the sensing gate V_{SG} [see Fig. 1(c)]. The other gate of the QPC is connected only to a voltage source, V_{CG}. The device and resonator chip are packaged and mounted in a dilution refrigerator with base temperature $T \sim 20$ mK. The reflected rf response $\Gamma = |\Gamma|e^{i\phi}$ from the sensing gate is amplified at the 4-K stage of the refrigerator and again at room temperature, where it is demodulated to yield amplitude Γ and phase ϕ components using a vector-network analyzer (VNA).

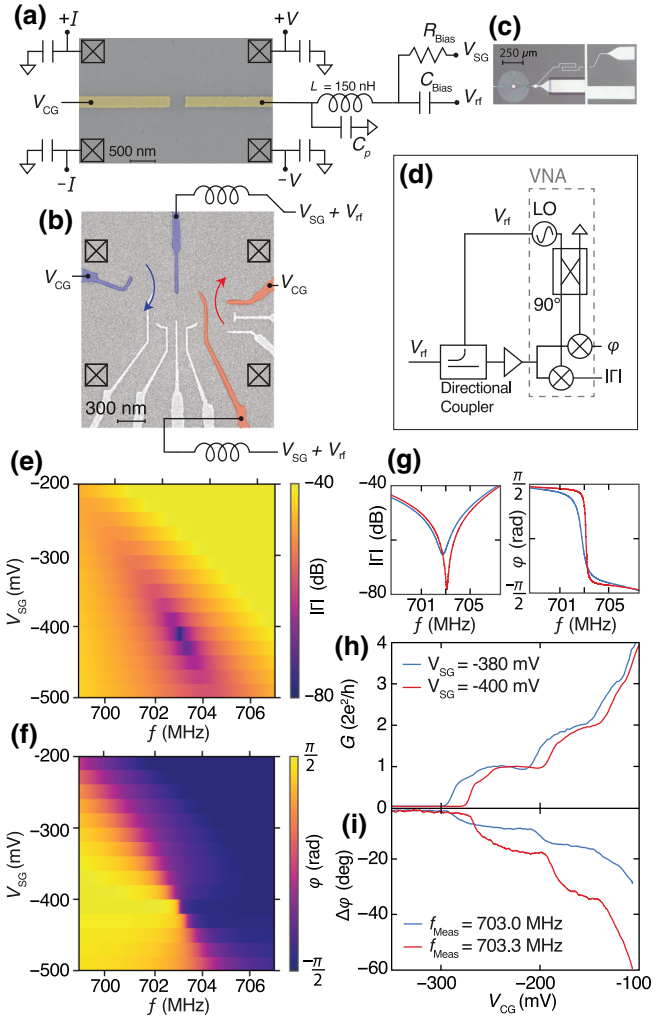

FIG. 1. (a) A micrograph of two distinct device gate patterns, showing QPCs formed in between two metallic gate electrodes. Device 1 has the pattern shown in (a), whereas device 2 (blue gates) and device 3 (red gates) are configured with the gate pattern shown in (b). For each device, one gate is bonded to a resonator comprising an inductor L, in resonance with the parasitic capacitance of the device, C_p. (c) A photograph of the off-chip resonator, in which a bias tee also allows a negative voltage to be applied to the gate. (d) The measurement setup, showing a cryogenic amplification and a demodulation circuit. The demodulated magnitude $|\Gamma|$ and phase ϕ responses are read out by a network analyzer. For device 1, (e) $|\Gamma|$ and (f) ϕ as a function of V_{SG} and the frequency f near resonance. (g) $|\Gamma|$ and ϕ at $V_{SG} = -380$ mV (blue) and -400 mV (red), with varying Q factors of approximately 1100 and 4200, respectively. (h) The conventional zero-bias conductance measurement for the two values of V_{SG}. (i) The change in the demodulated phase response $\Delta\phi$ for the same swept V_{CG} range as (h), taken at $f_{Meas} = 703.0$ MHz (red) and 703.3 MHz (blue) to maximize the dynamic range.

Focusing first on the classic split-gate QPC geometry of device 1 [Fig. 1(a)], we bias V_{SG} negatively to deplete

the 2DEG underneath the gate and reduce the 2D geometric capacitive contribution of the resonator. Lowering the capacitance increases the resonance frequency f_0, [as shown in $|\Gamma|$ in Figs. 1(e) and ϕ in 1(f)] and also changes the quality factor of the resonator by altering its impedance match with respect to the characteristic impedance of the transmission line ($Z_0 = 50\ \Omega$). Ideally, we wish to independently adjust f_0 and the match to the feed line to ensure maximum sensitivity. Similar to approaches that exploit varactors to tune the response of a resonator [24,25], we make use of an additional parallel resonator that is part of our frequency multiplexing chip [23] to partially tune the matching between the resonator and the feed line. Here, the additional resonator is also bonded to a gate elsewhere on the chip such that it acts as a voltage-controlled capacitor. This approach works since (depending on its capacitance) the parallel resonator can be configured to slightly overlap in frequency with the DGS resonator. With device 1 set up in this way, the DGS resonator is measured for two different values of V_{SG} in Fig. 1(g), reaching a maximum Q factor of approximately 4200.

Continuing with device 1, for each of these two values of V_{SG}, a four-terminal measurement of the conductance G through the QPC is performed, as a function of V_{CG}. Familiar conductance plateaus, quantized in units of $2e^2/h$, are seen in Fig. 1(h). After electrically disconnecting the ohmic contacts from all current and voltage sources, the equivalent sweep is performed for a measurement of $\Delta\phi$, shown in Fig. 1(i). Inflections are observed in the phase response of the resonator at gate voltages corresponding to risers in the conductance. We attribute these inflections to the changing DOS in QPC with the gate voltage. We note that the sensitivity of the technique decreases over an extended gate voltage, since the changing quantum capacitance leads to a detuning in the resonator away from the frequency tone of our oscillator. A feedback circuit between the oscillator frequency and resonator response can extend the range and sensitivity of the measurement, adjusting the tone frequency to compensate for changes in capacitance.

Having demonstrated that a jump in the phase response ϕ of the resonator somewhat lines up with corresponding features in conductance, we switch to examine the QPC on device 2, which, despite its more complex geometry, produces a slightly larger signal (perhaps because of the reduced parasitic capacitance that arises from its thinner gates). For these measurements, we hold the dc voltage on V_{SG} at -1.25 V and sweep V_{CG}. The phase response of the resonator can be converted to a change in capacitance of the circuit for a fixed inductance ($L = 400$ nH), as shown by the red dots in Fig. 2(a). It is immediately striking that there is a correspondence between the detected change in capacitance and the familiar steps in conductance [shown in the inset of Fig. 2(a)]. This correspondence suggests that we are indeed detecting jumps in

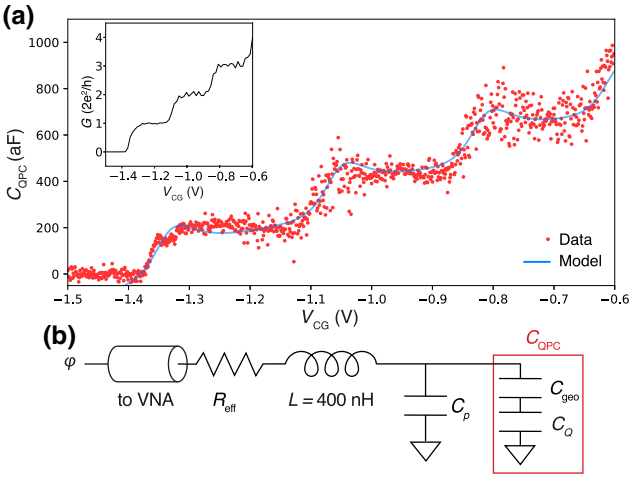

FIG. 2. (a) The dispersive response of device 2, converted to units of capacitance assuming a fixed inductance of $L = 400$ nH (red data points). The blue line is C_{QPC}, calculated using a simple model for the capacitance of a 1D system. The model includes contributions from the quantum C_Q as well as geometric C_{geo} capacitances, as shown by the simplified equivalent circuit in (b). Here, C_p is the parasitic capacitance to ground that also includes the geometric capacitance of the gate electrode in the region far from the QPC. See the main text for further details.

the quantum capacitance of the 1D region as each sub-band populates.

To gain further insight into these jumps, we estimate the capacitance, C_{QPC} using a simple model for a 1D system, noting that it comprises the series summation of two terms, the geometric capacitance C_{geo} between the gate and the QPC and the quantum capacitance C_Q, which accounts for the arrangement of charge in the QPC [26] [for an equivalent circuit, see Fig. 2(b)]. This capacitance can be estimated as $C_Q \sim l \times e^2 dN/d\mu$, where l is the length of the 1D region, μ is the chemical potential set by the gate voltage, and the density N is the integral over the 1D DOS multiplied by the transmission probability of occupying a state: $N = \int \rho(\mu)T(\mu)d\mu$, where $T(\mu) \sim 1/(1 + e^{-\pi\epsilon_j})$ depends on the ratio of ω_y/ω_x. Using the standard form of the DOS for a 1D system at zero temperature [17], $\rho(\mu) = g_s \sum_{j=0}^{n} \sqrt{m^*/2\hbar^2\pi^2(\mu - E_j)}$, (where jth indexes the sub-band, E_j is the jth sub-band edge, g_s is the spin degeneracy, and m^* is the effective mass), we calculate the probability that a state is occupied using the energy spectrum of the saddle-point potential of the QPC, as described for conductance in Ref. [27]. Allowing for channels that are neither completely open nor closed, the transmission coefficient $T(\mu)$ (see Ref. [27]) leads to tunnel broadening of the capacitive response C_Q in a similar way to the transitions between conductance plateaus. As in Ref. [27], we estimate the ratio of the saddle-point energies ($\omega_y/\omega_x \sim 3$) from the widths of the conductance plateaus

and transitions, and using the lever arm extracted from bias spectroscopy ($\Delta V_{CG} = 100$ mV/$\Delta V_{SD} = 0.75$ mV), we convert the gate voltage to energy and calculate C_{QPC}, shown as the blue line in Fig. 2(a). The model also includes a linear term (approximately 0.75 fF/V) to account for the dependence of C_{QPC} with the gate voltage that arises from the depletion of the electron gas under the gate (but away from the 1D region).

Comparing this simple model to the data in Fig. 2(a), we now conclude that the jumps in the measured quantum capacitance relate to the sudden increase in available states each time the chemical potential crosses into the next 1D sub-band. The sharp Van Hove singularities in the 1D DOS, however, are broadened in the capacitive response on account of tunneling into the QPC (the finite temperature and rf power also contribute to additional broadening). It is also worth noting that the gate sensor likely averages the response of the 1D DOS with some contributions from the 2D source and drain reservoirs, i.e., averaging the Van Hove singularity with the constant DOS from the 2D regions. Nevertheless, even accounting for broadening, we can state that the DGS technique is able to probe the local DOS of the 1D region, which contributes a quantum capacitance of roughly 200 aF per 1D sub-band for an approximately 200 nm long QPC. We also note that the capacitance data also indicate a feature below the first sub-band that is usually associated with the so-called 0.7 anomaly [28].

III. DISPERSIVE GATE SENSING AND TRANSPORT COMPARISON

Returning to the split-gate QPC (device 1), we now examine the regime of finite bias, where a source-drain voltage can be used to perform spectroscopy of the QPC sub-bands [29], noting differences between transport measurements and the DGS technique. It is worth stating that the two techniques are somewhat distinct, since with transport the QPC potential is only weakly perturbed as the chemical potential either side is varied and probed by a small oscillating voltage. Alternatively, in the case of DGS, the gate-defined QPC potential is made to oscillate up and down in energy at the resonance frequency as the dc bias is held constant. In any case, both the derivative of the ac conductance, dG/dV_{CG}, and the derivative of the phase response of the DGS, $d\phi/dV_{CG}$, exhibit familiar features associated with the 1D sub-bands, even though the capacitance is not quantized. Similarity between the measurements can be seen in the structures near zero bias and bias values that correspond to the source and drain potentials differing by a sub-band (the so-called finite-bias half-plateaus [29]).

A notable difference between transport and DGS is the asymmetry in the features that occur near pinch-off about zero bias, shown as cut along the red dashed line at $V_{CG} =$

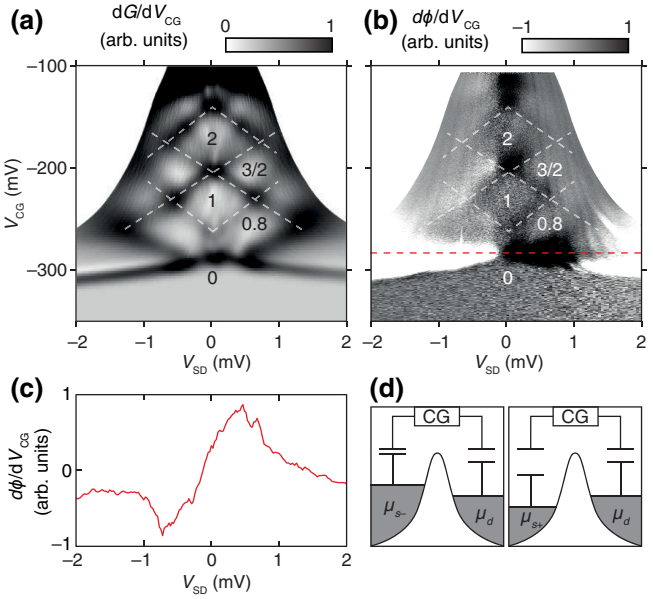

FIG. 3. Bias spectroscopy of device 1's QPC. (a) Transconductance and (b) differentiated reflected phase response. (c) A slice through $d\phi/d_{VCG}$ at $V_{CG} = -285$ mV (red dashed line), showing a peak at negative bias and trough at positive bias, indicating that the phase response is sensitive to asymmetric application of bias. (d) A sketch of the source-drain reservoirs relative to one another as the bias is changed. The potential of μ_d remains constant, while the potential of μ_s moves above and below it, changing the capacitive coupling between it and the confining gate.

-285 mV in Fig. 3(b). Peaks (black) occur at negative bias and troughs (white) occur at positive bias in $d\phi/dV_{CG}$, as shown in Fig. 3(c). We attribute this apparent change in the sign of $d\phi/dV_{CG}$ to the asymmetric configuration of the source-drain bias relative to the potential of the gate, when a tunnel barrier disconnects the reservoirs either side of the QPC (see the Appendix). While the drain potential μ_d is held at ground, the source potential μ_s is raised and lowered, changing the capacitive coupling to the sensing gate, as shown schematically in Fig. 3(d).

IV. DGS IN THE STRONGLY PINCHED-OFF REGIME

Finally, we apply the DGS technique to a third device (device 3) that has a gate pattern nominally identical to that of device 2 but contains additional features in its capacitive response. Here, we form a QPC with the gates shaded red in Fig. 1(b), a configuration that is commonly used to define a spin qubit based on a double-dot potential. Such a gate geometry has been used extensively for charge-sensing double dots when the QPC is biased near pinch-off [30]. The saddle-point potential of the QPC in this gate configuration is likely not as clean as the classic "split-gate" arrangement examined earlier, since the QPC

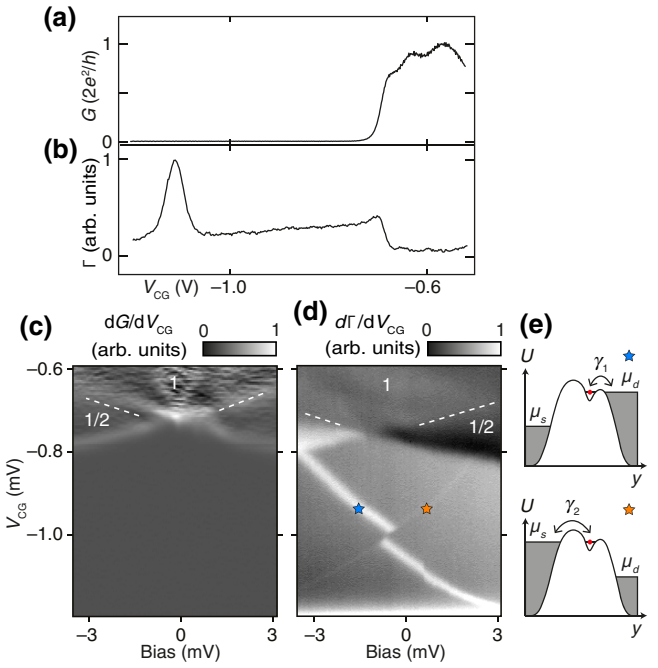

FIG. 4. Device 3 with an asymmetric QPC geometry, as commonly used for spin qubit experiments [Red gates in Fig. 1(b)]. V_{SG} and V_{CG} perform identical functions as before, resonator frequency is 545.5 MHz. (a) The conductance and (b) the DGS response over the same swept range of V_{CG}. A large peak occurs past pinch-off, at approximately $V_{CG} = -1150$ mV, visible only in the DGS response. The bias spectroscopy of the asymmetric QPC (device 3), (c) the transconductance and (d) the differentiated DGS response, showing the evolution of the peak with bias. There is a stray offset bias of approximately −0.5 mV across the device. (e) A sketch depicting a cross section of the QPC saddle-point potential, controlled with the gate voltage, relative to the source and drain energy. The data in (d) are consistent with an unintentional quantum dot forming in the QPC past pinch-off, with different tunnel rates $\gamma_{1,2}$ to the reservoirs as indicated by the symbols.

conductance does not exhibit a clear quantized staircase [31].

Again, we compare transport measurements to the response of the DGS, as shown in Figs. 4(a) and 4(b). At the point at which the QPC begins to open, the DGS response mirrors the step change seen in conductance but, in contrast to transport, it shows the appearance of a large additional peak, far beyond the gate voltage needed to pinch off the QPC.

To investigate this anomaly further, we perform bias-spectroscopy measurements, plotting the conductance and the DGS response side by side in Figs. 4(c) and 4(d). Although the features in conductance are not clean, it is possible to make out the first plateau and the first subband edge before pinch-off. In contrast, DGS clearly shows two diagonal features, one stronger than the other, that cross (or potentially anticross) near zero bias. We attribute these features to the presence of an unintentional quantum dot or charge pocket [20], formed in (or very close to) the QPC saddle potential [see the sketch in Fig. 4(e)]. In this sense, the diagonal lines correspond to the typical bias diamonds of Coulomb blockade. Note that in this regime of deep pinch-off, the tunnel barrier is raised well above the potential of the source or drain, making it impossible to perform transport measurements. It is unknown if this charge pocket is a genuine trap or, rather, a local minimum in the potential stemming from the complicated nonadiabatic constriction imposed by this T-shaped gate pattern. Again, we recognize that the DGS technique is sensitive to changes in the local DOS and holds promise as a means of investingating disorder in the surrounding potential landscape.

ACKNOWLEDGMENTS

This work was supported by the ARC via the Centre of Excellence in Engineered Quantum Systems (EQuS) (Grants No. CE110001013 and No. CE170100009) and the Microsoft Corporation. We thank S. J. Pauka and X. G. Croot for technical assistance and discussions,

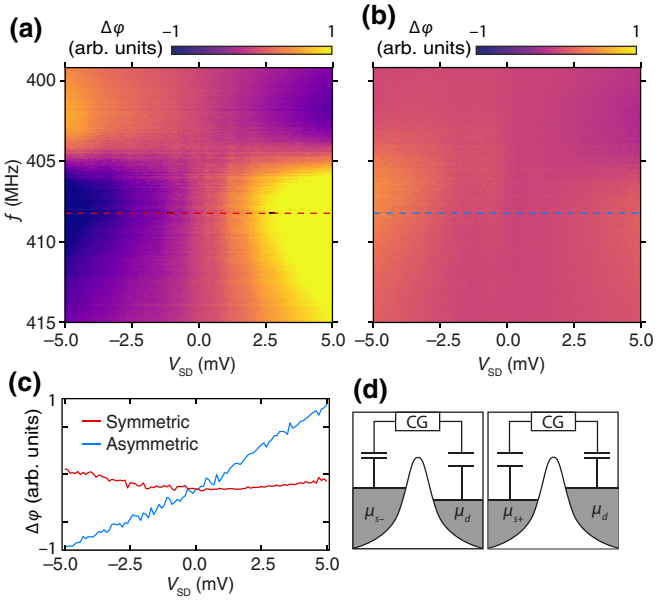

FIG. 5. We further explore the phase response as a function of the frequency for (a) asymmetric and (b) symmetric applications of source-drain bias, normalized to the response at zero bias. The color scale remains the same between the two plots. Asymmetric application reveals peaks and troughs similar to our measurement, while symmetric application does not. (c) If we take a cut at 408 MHz, we observe a global slope in the phase response about the device for asymmetric application (blue), but not for symmetric application (red). (d) The schematic of the reservoir potentials for symmetric bias, analogous to that presented for asymmetric bias in Fig. 3(d).

J. M. Hornibrook for the development of the frequency multiplexing chip, and J. I. Colless for the fabrication of the asymmetric QPC device.

APPENDIX: COMPARING ASYMMETRIC AND SYMMETRIC APPLICATION OF BIAS

Here, we explore the effect of bias application on the phase response. Rather than using bias spectroscopy, we measure how the response changes as a function of frequency, dependent on the relative potential of the source and drain reservoirs. Asymmetric application, where one reservoir is grounded (as in the text), is shown in Fig. 5(a), where the phase response is normalized to that at zero bias. As in the text, peaks and troughs occur about zero bias. In contrast, symmetric application, where the bias is split across the two ohmics, is shown in (b). This time, there is no discernible difference in the response about zero bias. If we take a cut at 408 MHz in (c), we can see a global slope in the phase response as a function of asymmetric bias, due to the constant change in the capacitive coupling to the reservoirs. This does not occur for symmetric bias, the equivalent schematic for which is shown in (d), analogous to that presented in Fig. 3(d).

[1] B. J. van Wees, H. van Houten, C. W. J. Beenakker, J. G. Williamson, L. P. Kouwenhoven, D. van der Marel, and C. T. Foxon, Quantized Conductance of Point Contacts in a Two-Dimensional Electron Gas, Phys. Rev. Lett. **60**, 848 (1988).

[2] D. A. Wharam, T. J. Thornton, R. Newbury, M. Pepper, H. Ahmed, J. E. F. Frost, D. G. Hasko, D. C. Peacock, D. A. Ritchie, and G. A. C. Jones, One-dimensional transport and the quantisation of the ballistic resistance, J. Phys. C: Solid State Phys. **21**, L209 (1988).

[3] M. Büttiker, A. Prêtre, and H. Thomas, Dynamic Conductance and the Scattering Matrix of Small Conductors, Phys. Rev. Lett. **70**, 4114 (1993).

[4] R. C. Ashoori, H. L. Stormer, J. S. Weiner, L. N. Pfeiffer, S. J. Pearton, K. W. Baldwin, and K. W. West, Single-Electron Capacitance Spectroscopy of Discrete Quantum Levels, Phys. Rev. Lett. **68**, 3088 (1992).

[5] K. D. Petersson, C. G. Smith, D. Anderson, P. Atkinson, G. A. C. Jones, and D. A. Ritchie, Charge and spin state readout of a double quantum dot coupled to a resonator, Nano Lett. **10**, 2789 (2010).

[6] M. D. Schroer, M. Jung, K. D. Petersson, and J. R. Petta, Radio Frequency Charge Parity Meter, Phys. Rev. Lett. **109**, 166804 (2012).

[7] S. J. Chorley, J. Wabnig, Z. V. Penfold-Fitch, K. D. Petersson, J. Frake, C. G. Smith, and M. R. Buitelaar, Measuring the Complex Admittance of a Carbon Nanotube Double Quantum Dot, Phys. Rev. Lett. **108**, 036802 (2012).

[8] J. Verduijn, M. Vinet, and S. Rogge, Radio-frequency dispersive detection of donor atoms in a field-effect transistor, Appl. Phys. Lett. **104**, 102107 (2014).

[9] F. Pei, Doctoral thesis, Delft University of Technology (2015).

[10] P. Scarlino, D. J. van Woerkom, A. Stockklauser, J. V. Koski, M. C. Collodo, S. Gasparinetti, C. Reichl, W. Wegscheider, T. Ihn, K. Ensslin, and A. Wallraff, All-Microwave Control and Dispersive Readout of Gate-Defined Quantum Dot Qubits in Circuit Quantum Electrodynamics, Phys. Rev. Lett. **122**, 206802 (2019).

[11] X. Mi, M. Benito, S. Putz, D. M. Zajac, J. M. Taylor, G. Burkard, and J. R. Petta, A coherent spin-photon interface in silicon, Nature **555**, 599 (2018).

[12] D. de Jong, J. van Veen, L. Binci, A. Singh, P. Krogstrup, L. P. Kouwenhoven, W. Pfaff, and J. D. Watson, Rapid Detection of Coherent Tunneling in an InAs Nanowire Quantum Dot through Dispersive Gate Sensing, Phys. Rev. Appl. **11**, 044061 (2019).

[13] J. I. Colless, A. C. Mahoney, J. M. Hornibrook, A. C. Doherty, H. Lu, A. C. Gossard, and D. J. Reilly, Dispersive Readout of a Few-Electron Double Quantum Dot with Fast rf Gate Sensors, Phys. Rev. Lett. **110**, 046805 (2013).

[14] A. West, B. Hensen, A. Jouan, T. Tanttu, C.-H. Yang, A. Rossi, M. F. Gonzalez-Zalba, F. Hudson, A. Morello, D. J. Reilly, and A. S. Dzurak, Gate-based single-shot readout of spins in silicon, Nat. Nanotechnol. **14**, 437 (2019).

[15] A. Rossi, R. Zhao, A. S. Dzurak, and M. F. Gonzalez-Zalba, Dispersive readout of a silicon quantum dot with an accumulation-mode gate sensor, Appl. Phys. Lett. **110**, 212101 (2017).

[16] J. Martin, B. E. Feldman, R. T. Weitz, M. T. Allen, and A. Yacoby, Local Compressibility Measurements of Correlated States in Suspended Bilayer Graphene, Phys. Rev. Lett. **105**, 256806 (2010).

[17] S. Ilani, L. A. K. Donev, M. Kindermann, and P. L. McEuen, Measurement of the quantum capacitance of interacting electrons in carbon nanotubes, Nat. Phys. **2**, 687 (2006).

[18] G. D. Mahan, *Many-Particle Physics* (Springer-US, New York, 2000).

[19] S. Lüscher, L. S. Moore, T. Rejec, Y. Meir, H. Shtrikman, and D. Goldhaber-Gordon, Charge Rearrangement and Screening in a Quantum Point Contact, Phys. Rev. Lett. **98**, 196805 (2007).

[20] X. Croot, S. Pauka, M. Jarratt, H. Lu, A. Gossard, J. Watson, G. Gardner, S. Fallahi, M. Manfra, and D. Reilly, Gate-Sensing Charge Pockets in the Semiconductor-Qubit Environment, Phys. Rev. Appl. **11**, 064027 (2019).

[21] T. Karzig, C. Knapp, R. M. Lutchyn, P. Bonderson, M. B. Hastings, C. Nayak, J. Alicea, K. Flensberg, S. Plugge, Y. Oreg, C. M. Marcus, and M. H. Freedman, Scalable designs for quasiparticle-poisoning-protected topological quantum computation with Majorana zero modes, Phys. Rev. B **95**, 235305 (2017).

[22] D. Pikulin, K. Flensberg, L. I. Glazman, M. Houzet, and R. M. Lutchyn, Coulomb Blockade of a Nearly Open Majorana Island, Phys. Rev. Lett. **122**, 016801 (2019).

[23] J. M. Hornibrook, J. I. Colless, A. C. Mahoney, X. G. Croot, S. Blanvillain, H. Lu, A. C. Gossard, and D. J. Reilly, Frequency multiplexing for readout of spin qubits, Appl. Phys. Lett. **104**, 103108 (2014).

[24] N. Ares, F. J. Schupp, A. Mavalankar, G. Rogers, J. Griffiths, G. A. C. Jones, I. Farrer, D. A. Ritchie, C. G. Smith, A. Cottet, G. A. D. Briggs, and E. A. Laird, Sensitive Radio-Frequency Measurements of a Quantum Dot by Tuning to Perfect Impedance Matching, Phys. Rev. Appl. **5**, 034011 (2016).

[25] D. J. Ibberson, L. A. Ibberson, G. Smithson, J. A. Haigh, S. Barraud, and M. F. Gonzalez-Zalba, Low-temperature tunable radio-frequency resonator for sensitive dispersive readout of nanoelectronic devices, Appl. Phys. Lett. **114**, 123501 (2019).

[26] J. Gabelli, G. Fève, J.-M. Berroir, B. Plaçais, A. Cavanna, B. Etienne, Y. Jin, and D. C. Glattli, Violation of Kirchhoff's laws for a coherent *RC* circuit, Science **313**, 499 (2006).

[27] M. Büttiker, Quantized transmission of a saddle-point constriction, Phys. Rev. B **41**, 7906 (1990).

[28] D. J. Reilly, Phenomenological model for the 0.7 conductance feature in quantum wires, Phys. Rev. B **72**, 033309 (2005).

[29] N. K. Patel, J. T. Nicholls, L. Martn-Moreno, M. Pepper, J. E. F. Frost, D. A. Ritchie, and G. A. C. Jones, Evolution of half plateaus as a function of electric field in a ballistic quasi-one-dimensional constriction, Phys. Rev. B **44**, 13549 (1991).

[30] D. J. Reilly, C. M. Marcus, M. P. Hanson, and A. C. Gossard, Fast single-charge sensing with a rf quantum point contact, Appl. Phys. Lett. **91**, 162101 (2007).

[31] This is true not just for the device examined here but for many devices that we have measured with this gate pattern.